ACS Photonics

Article

pubs.acs.org/journal/apchd5

Observation of Nanoscale Refractive Index Contrast via Photoinduced Force Microscopy

Antonio Ambrosio,*[,†,‡,§] Robert Charles Devlin,[‖] Federico Capasso,[‖] and William L. Wilson*[,†]

[†]Center for Nanoscale Systems, [‡]Department of Physics, and [‖]Harvard John A. Paulson School of Engineering and Applied Sciences, Harvard University, Cambridge, Massachusetts 02138, United States

[§]CNR-SPIN U.O.S. Napoli, Complesso Universitario di Monte Sant'Angelo, Via Cintia, 80126 − Napoli, Italy

Supporting Information

ABSTRACT: Near-field optical microscopy (NSOM) is a scanning probe technique that allows optical imaging of sample surfaces with nanoscale resolution. Generally, all NSOM schemes rely on illuminating the sample surface and collecting the localized scattered light resulting from the interaction of the microscopes nanoscale probe with the sample surface in the illuminated region. Currently, a new set of nanospectroscopic techniques are being developed using Atomic Force Microscopes to detect optical interactions without detecting any light. One of these approaches is photoinduced force microscopy (PiFM), where local optical forces, originated by the illumination of the tip−sample region, are mechanically detected as forced oscillations of the cantilever of an atomic force microscope operating in a multifrequency mode. In this article we show high resolution nanoimaging via PiFM with a contrast only related to the local refractive index of a sample specifically designed to unambiguously decouple morphology from optical response at the nanoscale. Imaging lateral resolution better than 10 nm is obtained, and the optimization of the contrast mechanism is described. Our results represent a step forward in understanding the potential of the PiFM technique, showing the possibility of high resolution imaging of the local polarizability of the sample and subsequently using the mechanism to explore complex spectral behavior at the nanoscale.

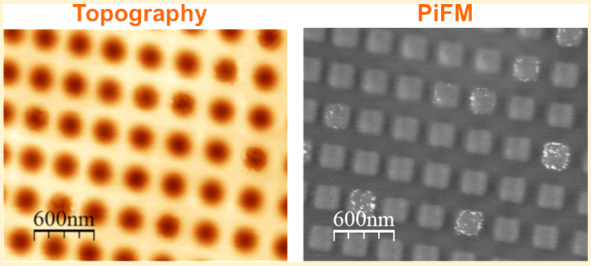

KEYWORDS: *photoinduced force microscopy, near-field optical microscopy, multifrequency atomic force microscopy*

Atomic force microscopy (AFM) has become one of the most valuable and versatile techniques for the nanoscale characterization of material surfaces, particularly in terms of roughness and morphology.[1,2] The possibility of detecting a wide variety of physical phenomena via forces due to the local interactions between samples' surface and various optimized AFM probes has led to many variations of the technique ranging from electric force microscopy[3,4] (EFM) and magnetic force microscopy[5,6] (MFM), to microwave impedance microscopy.[7,8] These methods allow generation of high-resolution maps of specific materials properties (charge density, magnetic domains, permittivity, etc.) with sub 50 nm resolution.[9,10] Recently there has been an increasing interest in approaches enabling AFM based optical spectroscopy.[11] The advancement in these techniques have been fueled by developments in multifrequency atomic force microscopy enabling detection of weak molecular forces with nanoscale spatial resolution.[12−14] Today there are a number of different recent experimental schemes trying to use the sensitivity of AFM probes to detect light-driven local forces on the sample surface.[15−17] These approaches enable a pure mechanical detection of the optical properties of the samples, that is, the absorption spectrum of molecules, spectral dynamics, and so on.

The detection of weak local mechanical forces is routinely achieved in multifrequency AFM where the cantilever, operated in tapping mode, can oscillate on more than one flexural mode (eigenmodes), each at a specific frequency (Figure 1). Typical examples are cantilevers whose first flexural mode is approximately ω_0 = 270 kHz with the second eigenmode at ω_1 = 6.6 ω_0 (i.e., 1.8 MHz). To image in "bimodal" AFM, for example, the first mode is used as the control in the feedback loop to maintain the tip−sample working distance during scanning, while the second mode parameters, (amplitude, phase, and possibly frequency) are modified by the tip−sample interaction forces, providing enhanced contrast for imaging materials properties. Here we discuss imaging via photoinduced force microscopy (PiFM), a scanning probe technique developed around a bimodal AFM.[18,19] The technique is unique in that it allows measurement of the photoinduced polarization generated in the specimen below the tip as a local mechanical force. The result is an imaging contrast related directly to the local polarizability of the sample.

In PiFM, as in bimodal, one of the oscillation eigenmodes of the cantilever is used in the feedback loop to set the tip−sample working distance, that is, the effective z position. The other

Received: November 15, 2016
Published: March 21, 2017

DOI: 10.1021/acsphotonics.6b00911
ACS Photonics XXXX, XXX, XXX−XXX

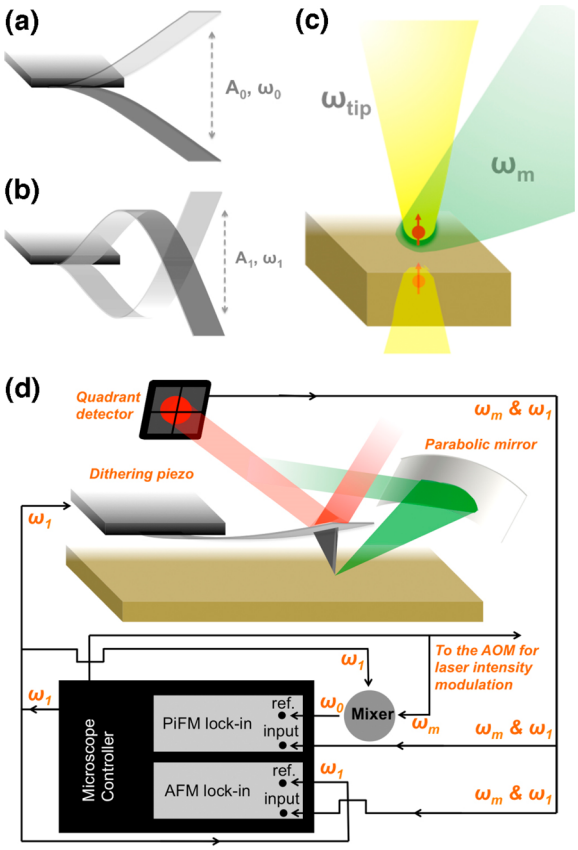

Figure 1. (a) Schematic representation of an AFM cantilever oscillation corresponding to its first eigenmode at frequency ω_0. (b) Schematic representation of an AFM cantilever oscillation corresponding to its second eigenmode at frequency $\omega_1 \approx 6.6\omega_0$. (c) A metal-coated AFM tip oscillates in a tapping mode AFM at frequency ω_{tip}. A laser (532 nm wavelength) is focused on the tip/sample volume and is modulated at frequency ω_m. (d) Schematic of the setup. A green laser (532 nm wavelength) is focused by means of a parabolic mirror onto the sample surface and an AFM probe in a side-illumination scheme. The quadrant photodiode of the AFM provides an electric signal that is modulated at ω_m and ω_1. The signal is split and demodulated by two lock-in amplifiers. One lock-in has ω_1 as reference and is used to extract the oscillation amplitude and phase of the second eigenmode, used for topography feedback. The other lock-in has a reference at ω_0 provided by a mixer where the signal at ω_m combines with a reference at ω_1. This lock-in amplifier detects the amplitude of the optical-near-field-driven cantilever oscillations (PiFM signal).

mode is instead excited by the sample-tip interaction driven by an external light source. More specifically, a laser beam is focused on the sample from the side (or from the bottom) illuminating the tip−sample interface (Figure 1c). Similar to a scattering near-field optical microscope (s-NSOM),[20−24] the illuminating light induces an oscillating dipole at the tip end that triggers an interaction between the induced dipole in the tip and its mirror image in the sample. This interaction is nonlinear with respect to the distance z from the sample surface. In s-NSOM the nonlinearity is used to isolate the optical near-field scattered below the tip from the light background generated from far-field scattering and reflections from the cantilever and the sample. However, the optical near-field also contributes (optical force) to the local force experienced by the tip of the AFM. Thus, by modulating the laser at the frequency of the cantilever eigenmode, not used for feedback in the AFM controller, results in mechanically resonant dipole-coupled light-driven oscillations of the cantilever. Such oscillations are monitored as an electrical signal from a quadrant photodiode by means of a lock-in amplifier (standard position sensitive circuit of AFMs to monitor the cantilever deflection; Figure 1d). These additional mechanical signals are proportional to the optical force exerted by the near-field on the AFM tip. The tip, in essence acts as a nonlinear mixer detecting all the induced mechanical oscillations created at the sample surface. Isolating the signal at the frequency of interest and plotting the optical force while scanning the AFM tip on the surface, allows building a near-field image without detecting any light. This is the working principle of PiFM, it highly simplifies near-field imaging, eliminating limitations related to far-field background.[25−29]

To further clarify how the signals are processed, it is worth describing the specific experimental setup (Figure 1d). Our setup is based on a commercial microscope platform (Molecular Vista). A green laser (532 nm wavelength) is focused by means of a parabolic mirror onto the sample surface and AFM probe in a side-illumination scheme. This laser beam is the first diffraction order from an acousto-optic modulator (AOM) driven at the frequency of interest. In our microscope, the tip-to-sample stabilization is obtained through feedback on the second eigenmode of the cantilever ($\omega_1 \approx 1.8$ MHz). The flexure mode used to detect the photoinduced force is instead the first mode $\omega_0 \approx 270$ kHz. This operating scheme is used to dither the cantilever with smaller oscillations (the second eigenmode has higher Q-factor) and to ensure that the probe stays closer to the sample surface where the near-field interaction is stronger (~10 nm). In addition, the illuminating laser is not modulated directly at ω_0 but at $\omega_m = \omega_1 \pm \omega_0$ (frequency sum or difference). The quadrant photodiode of the AFM provides an electric signal that is modulated at ω_m and ω_1. The signal is first split and then demodulated by two lock-in amplifiers. One lock-in has ω_1 as reference and is used to extract the oscillation amplitude and phase of the second eigenmode (used for topography feedback). The other lock-in has a reference at ω_0 provided by a mixer where the signal at ω_m combines with a reference at ω_1. This lock-in amplifier detects the amplitude of the optical near-field-driven cantilever oscillations (PiFM signal). As further discussed below, this operating scheme, called sideband detection, results in a better signal-to-noise ratio and improves the signal localization by suppressing the detection of nonconservative optical forces (scattering force), which also effect the tip oscillation.[30]

Below, we describe how we obtain nanometric-resolution pure refractive index contrast imaging by means of PiFM on dielectric nanostructures made of TiO_2. These nanostructured samples allow us to gain important insights into the fundamental physics of the technique as well as its resolution limits. The sample consists of a 2D array of titanium dioxide (TiO_2) squares, with each square 200 nm × 200 and 350 nm tall, embedded in a matrix of electron beam resist (ZEP 520A, ZEON Corp.; Figure 2). In one direction, the array consists of 21 individual TiO_2 squares with an increasing gap between each successive square, ranging from 10 to 200 nm spacing between the first two and last two squares, respectively. In the orthogonal direction, the TiO_2 squares are offset from each other by a constant 200 nm.

To fabricate the structures, TiO_2 is directly deposited onto an exposed electron beam resist (EBR) pattern by means of atomic layer deposition (ALD). The substrate is fused silica (similar to ref 31). After ALD, an isotropic reactive ion etch

DOI: 10.1021/acsphotonics.6b00911
ACS Photonics XXXX, XXX, XXX−XXX

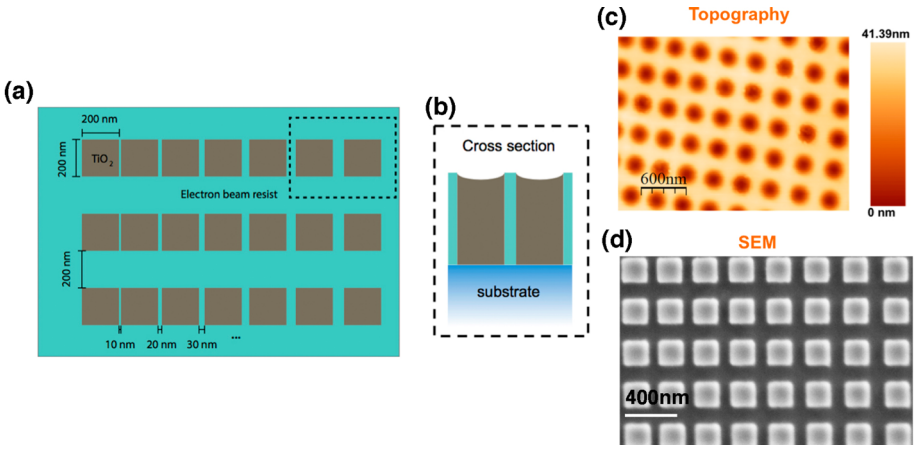

Figure 2. (a) Sample consists of an array of titanium dioxide (TiO_2) squares embedded in a matrix of electron beam resist (ZEP 520A, ZEON Corp.) on a fused silica substrate. In one direction, the array consists of 21 individual TiO_2 squares with an increasing gap between each successive square. In the orthogonal direction the TiO_2 squares are offset from each other by a constant distance. (b) Cross section of the TiO_2 structures. The sample is typically overetched by nominal 10−20 nm. This results into shallow hemispherical troughs in the surface morphology clearly seen in AFM topography (c). (d) SEM micrographs of the same sample showing the TiO_2 squares embedded in the ZEP matrix. From the SEM image, the TiO_2 squares are 230 nm × 230 nm, with 170 nm space between two rows.

step then follows to produce a nearly planar array of TiO_2 structures in the electron beam resist matrix. However, in order to ensure that the TiO_2 film overlayer deposited during the ALD step is completely removed and only the squares of TiO_2 and EBR remain, the sample is typically overetched by nominal 10−20 nm. This overetching causes in fact the tops of the TiO_2 squares to be slightly recessed with respect to the height of the EBR (see cross section in Figure 2b). This results in shallow hemispherical indentations in the surface morphology clearly seen in AFM topography (Figure 2c), where the squared structures of the TiO_2 are not visible. SEM micrographs of the same sample show the TiO_2 squares embedded in the ZEP matrix (Figure 2d). The ZEP and TiO_2 have very different contrast responses to the electron beam. This allows one to measure the effective sizes of the TiO_2 squares that are 230 nm × 230 nm, 170 nm space between two rows (Figure 2d).

Figure 3 shows the PiFM signal (amplitude of the optical-near-field-driven tip oscillation) image of our TiO_2 sample. Although the topography (collected simultaneously) cannot show the square nature of the TiO_2 structures, the PiFM image clearly shows the correct shape (and size) of the nanostructures, highlighting the TiO_2 features, whose refractive index at 532 nm wavelength is $n_{TiO_2} = 2.428$, much higher than that of the EBR, whose refractive index is $n_{EBR} = 1.56$ (note: both TiO_2 and ZEP have transmission higher than 87% at this wavelength, there is no intrinsic adsorption in this sample at 532 nm).[31] In fact, the time average optically driven force that originates the PiFM signal in sideband modulation can be approximately described as an interaction between the dipole induced at the tip end and its image-dipole in the sample[18,19] (Figure 1c). Under the assumption that the illuminating optical field is constant in the tip−sample surface region (distance below 10 nm) the local optical force (gradient force) can be approximated by the formula:[32]

$$F_{pot} \approx \frac{1}{Z^4}\mathrm{Re}\{\alpha_s \alpha_t^*\}|E_z|^2 \quad (1)$$

This formula reveals the main features of the local photo-induced force: the interaction is highly nonlinear and depends on z^{-4} (z is the distance between the tip and the sample); the

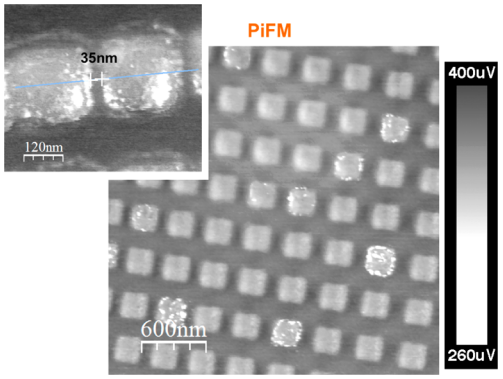

Figure 3. PiFM image of the TiO_2 squares embedded in ZEP photoresist. The PiFM signal is the amplitude from the lock-in amplifier demodulating at the first eigenmode frequency ω_0. The second eigenmode of the cantilever is instead used to retrieve the sample morphology and for tip-to-sample distance stabilization. The two materials have different refractive indices and are almost completely transparent to the illuminating light. Here the material with higher refractive index produces the lower PiFM signal. The figure's inset shows the PiFM image of a gap of 35 nm between two TiO_2 squared structures.

strength of the interaction depends upon the polarizability of both the tip (α_t) and the sample (α_s). This means that, once the tip material is fixed (we used platinum-coated tips), the interaction depends on the local material optical constants. This mechanism is responsible for the refractive index contrast shown in the PiFM image of Figure 3. The insert of Figure 3 shows a zoomed image of the gap between two squared TiO_2 structures. A gap as small as 35 nm is clearly distinguishable.

It is worth noting that the TiO_2 refractive index at λ = 532 nm is ≈1.6× that of ZEP. The PiFM signal from TiO_2 is instead ≈0.8× that obtained from the electron beam resist (in Figure 3, the features with higher refractive index (TiO_2 squares) show the lower PiFM signal). In fact, there are several conditions affecting the sign and strength of the contrast when operating PiFM in sideband modulation. Operating in direct mode, that is, when the modulation frequency of the illuminating laser directly matches the frequency of one of the eigenmodes of the

DOI: 10.1021/acsphotonics.6b00911
ACS Photonics XXXX, XXX, XXX−XXX

cantilever, it has been shown that quantitative information on the forces can be retrieved through fitting of force−distance curves.[18] As extensively discussed in ref 32, operating in direct-mode, has the drawback that at least another light-driven force, a nonlocal force (scattering force) is effective, producing an overall background to the signal of interest. In sideband modulation instead, the detection becomes sensitive almost exclusively to the local force described in eq 1.[33,34] This operating mode improves the signal-to-noise ratio allowing the high resolution imaging that we show here, but it makes difficult to absolutely quantify the detected signal. In fact in sideband modulation, where the laser modulation frequency is either $\omega_m = \omega_1 + \omega_0$ or $\omega_m = \omega_1 - \omega_0$, the optically induced oscillations on the tip also result in the modulation of the local force gradient (the gradient of the total local interaction force F, including mechanical (van der Waals, etc.) and optically induced forces) at the same frequency ω_m. The force gradient modulation induces a frequency shift ($\omega \rightarrow \omega'$) on the cantilever oscillation frequency according to the relation valid for small perturbations:[18]

$$\omega' = \sqrt{\left(k - \frac{\partial F}{\partial z}\right)/m} \tag{2}$$

where m is the effective mass and k is the effective stiffness (force constant) of the cantilever eigenmode. The continuous modulation of the force gradient at ω_m results in a frequency modulation which, together with the nonlinearity of the tip−sample interaction with the distance from the surface, produces sidebands at $\omega_1 \pm \omega_m$. In sideband modulation, $\omega_1 \pm \omega_m$ is adjusted to match one of the eigenmodes of the cantilever (the first mode in our experiment) and the PiFM signal is then dominated by the gradient of force in eq 1. This is actually why in sideband modulation the contribution of the scattering force is minimized. The scattering force is constant with respect to the tip−sample distance z and its gradient (derivative with respect to z) is in fact null. Reducing the nonlocal scattering force to negligible values strongly reduces the background and increase the signal-to-noise ratio.

However, the forces that contribute to the cantilever frequency shift described by eq 2 include also forces like van der Waals that depend on the material. As a result, the overall resonance frequency shift on one material can be different than that on another material. This may in practice influence the contrast in PiFM in a distinctive way. Figure 4 illustrates this concept. For this experiment, we used a standard glass coverslip that has unknown nanoparticles on its surface resulting from fabrication. Figure 4a shows the PiFM signal as a function of the illuminating laser modulation frequency. More precisely, the laser modulation is tuned around $\omega_m = \omega_1 - \omega_0$. The AFM topographical image of the sample surface is showed in Figure 4c. The free oscillation amplitude of the second eigenmode of the cantilever is less than 20 nm. The red curve in Figure 4a shows the PiFM signal vs demodulating frequency when the AFM feedback set point is at 81% (this means that the oscillation amplitude of the tip engaged with the surface is about 81% of the free oscillation amplitude) and the tip is on the glass coverslip. Note that the laser modulation frequency is also tuned accordingly. The blue curve in the same image shows instead the same signal when the tip is on one of the particles. In this case, the two peaks are shifted by only 2.7 kHz and the two curves are almost superimposed. Choosing either the peak of the blue or the red curve of Figure 4a as

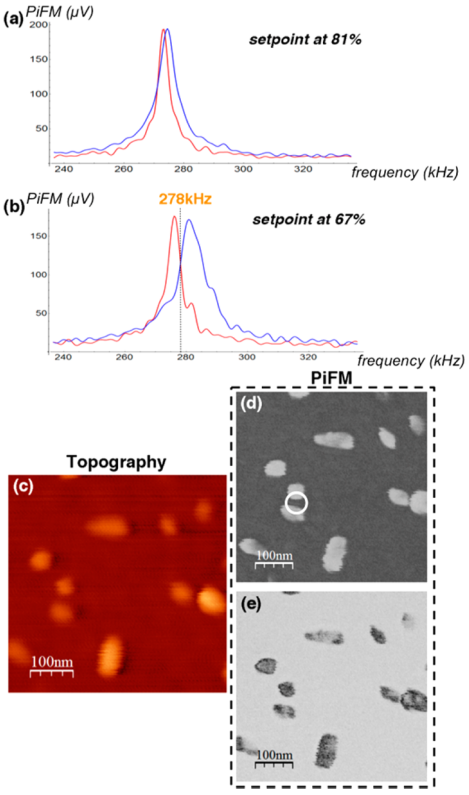

Figure 4. (a) PiFM signal as a function of the lock-in demodulating frequency (around the first eigenmode resonance). The red curve in (a) shows the PiFM vs demodulating frequency when the AFM feedback set point is at 81% and the tip is on the glass coverslip. The blue curve in the same image shows instead the same curve when the tip is on one of the particles. (b) Same as for (a) when the set point is 67%. (c) AFM topographical image of the sample surface. (d) PiFM image obtained when operating with 81% set point. (e) PiFM image obtained when the set point is changed to 67% and the laser modulation frequency and the lock-in demodulation frequency are both above 278 kHz.

demodulation frequency does not really matter in these conditions and it always results in a contrast where the PiFM signal is lower on the particles than on the glass (Figure 4d).

The contrast condition is quite different when the set point is changed from 81% to 67% (smaller tip−sample distance). Figure 4b shows the same curves of Figure 4a at this new working distance. Now, the red and blue curves, although quite similar in peak amplitudes, are shifted by 6.3 kHz. The two curves cross around 278 kHz. This means that when the demodulation frequency for the PiFM signal is set above 278 kHz, when the tip is on the particles the PiFM signal can be higher than when the tip is on the glass. This, in fact, results into a reversed contrast in the PiFM image, as shown in Figure 4e. When the lock-in demodulation frequency is set below 278 kHZ, the same contrast as in Figure 4d is re-established.

The possibility of reversing the contrast in PiFM imaging clearly shows that it is not possible, in such experimental conditions (sideband modulation), to extract any detailed quantitative information from the PiFM values on the optical parameters of the material. However, controlling the PiFM demodulation frequency, as described here, allows one to set conditions that maximize the contrast. This is crucial in imaging features like sharp edges shown in Figure 3 or small particles like those of Figure 4. It is worth noting that, in the PiFM

DOI: 10.1021/acsphotonics.6b00911
ACS Photonics XXXX, XXX, XXX−XXX

images of Figure 4, a gap between two features as small as 20 nm is easily detectable (white circle in Figure 4d). The minimum resolved gap in the same image is 5 nm only, that is, one of the smallest ever obtained in a near-field scanning probes experiment. It is also worth noting that the illuminating laser wavelength is 532 nm. It is challenging to use such short wavelength in s-NSOM that usually best performs in the mid-IR. Moreover, if the mechanical properties of the sample are uniform everywhere on the surface, we expect that quantitative information can be still extracted by comparing the PiFM signal on different surface features. This would be, for instance, the case of getting different PiFM values from different numbers of layers in 2D materials like MoS_2 or graphene. We are currently investigating these types of material systems.

In conclusion, we have shown that one can image directly refractive index contrast using PiFM with nanometric resolution. We specifically designed and fabricated a sample whose features allow us to completely and unambiguously decouple topography from the optical response related to the local refractive index. The absence of far-field light background enables nanometric resolution in the visible. This work suggests the significant potential of PiFM to explore complex optical behavior at the nanoscale.

■ ASSOCIATED CONTENT

Supporting Information

The Supporting Information is available free of charge on the ACS Publications website at DOI: 10.1021/acsphotonics.6b00911.

Amplitude and phase of the second eigenmodes of the cantilever during scanning of TiO_2 nanostructures. Brief description of the phase signal in the Photoinduced Force Microscopy imaging process (PDF).

■ AUTHOR INFORMATION

Corresponding Authors

*E-mail: ambrosio@seas.harvard.edu.
*E-mail: wwilson@cns.fas.harvard.edu.

ORCID

Antonio Ambrosio: 0000-0002-8519-3862

Notes

The authors declare no competing financial interest.

■ ACKNOWLEDGMENTS

This work is in part supported by Air Force Office of Scientific Research (MURI, Grants FA9550-16-1-0156). This work was performed in part at the Center for Nanoscale Systems (CNS), a member of the National Nanotechnology Coordinated Infrastructure (NNCI), which is supported by the National Science Foundation under NSF Award No. 1541959. CNS is a part of Harvard University.

■ REFERENCES

(1) Binnig, G.; Quate, C. F.; Gerber, C. Atomic Force Microscope. *Phys. Rev. Lett.* **1986**, *56*, 930−933.
(2) Binnig, G.; Gerber, C.; Stoll, E.; Albrecht, T. R.; Quate, C. F. Atomic Resolution with Atomic Force Microscope. *Surf. Sci.* **1987**, *189*, 1−6.
(3) Bohm, C. Electric force microscopy: Gigahertz and nanometer measurement tool. *Microelectron. Eng.* **1996**, *31*, 171−179.
(4) Yokoyama, H.; Inoue, T.; Itoh, J. Nonresonant Detection of Electric Force Gradients by Dynamic Force Microscopy. *Appl. Phys. Lett.* **1994**, *65*, 3143−3145.
(5) Hartmann, U. Magnetic Force Microscopy. *Adv. Mater.* **1990**, *2*, 550−552.
(6) Hartmann, U. Magnetic Force Microscopy - Some Remarks from the Micromagnetic Point of View. *J. Appl. Phys.* **1988**, *64*, 1561−1564.
(7) Seabron, E.; MacLaren, S.; Xie, X.; Rotkin, S. V.; Rogers, J. A.; Wilson, W. L. Scanning Probe Microwave Reflectivity of Aligned Single-Walled Carbon Nanotubes: Imaging of Electronic Structure and Quantum Behavior at the Nanoscale. *ACS Nano* **2016**, *10*, 360−368.
(8) Kundhikanjana, W.; Yang, Y.; Tanga, Q.; Zhang, K.; Lai, K.; Ma, Y.; Kelly, M. A.; Li, X. X.; Shen, Z. X. Unexpected surface implanted layer in static random access memory devices observed by microwave impedance microscope. *Semicond. Sci. Technol.* **2013**, *28*, 025010.
(9) Sugimoto, Y.; Pou, P.; Abe, M.; Jelinek, P.; Pérez, R.; Morita, S.; Custance, O. Chemical identification of individual surface atoms by atomic force microscopy. *Nature* **2007**, *446*, 64−67.
(10) Lai, C.-Y.; Santos, S.; Chiesa, M. Systematic multidimensional quantification of nanoscale systems from bimodal atomic force microscopy data. *ACS Nano* **2016**, *10*, 6265−6272.
(11) Atkin, J. M.; Berweger, S.; Jones, A. C.; Raschke, M. B. Nano-optical imaging and spectroscopy of order, phases, and domains in complex solids. *Adv. Phys.* **2012**, *61*, 745−842.
(12) Garcia, R.; Herruzo, E. T. The emergence of multifrequency force microscopy. *Nat. Nanotechnol.* **2012**, *7*, 217−226.
(13) Damircheli, M.; Payam, A. F.; Garcia, R. Optimization of phase contrast in bimodal amplitude modulation AFM. *Beilstein J. Nanotechnol.* **2015**, *6*, 1072−1081.
(14) Lozano, J. R.; Garcia, R. Theory of multifrequency atomic force microscopy. *Phys. Rev. Lett.* **2008**, *100*, 076102.
(15) Dazzi, A.; Prazeres, R.; Glotin, F.; Ortega, J. M. Local infrared microspectroscopy with sub-wavelength spatial resolution with an atomic force microscope tip used as a photothermal sensor. *Opt. Lett.* **2005**, *30*, 2388−2390.
(16) Lu, F.; Jin, M.; Belkin, M. A. Tip-enhanced infrared nanospectroscopy via molecular expansion force detection. *Nat. Photonics* **2014**, *8*, 307−312.
(17) Yang, H. U.; Rashcke, M. B. Resonant optical gradient force interaction for nano-imaging and − spectroscopy. *New J. Phys.* **2016**, *18*, 053042.
(18) Jahng, J.; Brocious, J.; Fishman, D. A.; Huang, F.; Li, X. W.; Tamma, V. A.; Wickramasinghe, H. K.; Potma, E. O. Gradient and scattering forces in photoinduced force microscopy. *Phys. Rev. B: Condens. Matter Mater. Phys.* **2014**, *90*, 155417.
(19) Huang, F.; Tamma, V. A.; Mardy, Z.; Burdett, J.; Wickramasinghe, H. K. Imaging Nanoscale Electromagnetic Near-Field Distributions Using Optical Forces. *Sci. Rep.* **2015**, *5*, 10610.
(20) Nikiforov, M.; Kehr, S. C.; Park, T.-H.; Milde, P.; Zerweck, U.; Loppacher, C.; Eng, L. M.; Therien, M. J.; Engheta, N.; Bonnell, D. Probing polarization and dielectric function of molecules with higher order harmonics in scattering-near-fireld optical microscopy. *J. Appl. Phys.* **2009**, *106*, 114307.
(21) Govyadinov, A. A.; Amenabar, I.; huth, F.; Carney, P. S.; Hillenbrand, R. Quantitative measurement of local infrared absorption and dielectric function with tip-enhanced near-field microscopy. *J. Phys. Chem. Lett.* **2013**, *4*, 1526−1531.
(22) Xu, X. G.; Tanur, A. E.; Wlaker, G. C. Phase controlled homodyne infrared near-field microscopy and spectroscopy reveal inhomogeneity within and anong individual boron nitride nanotubes. *J. Phys. Chem. A* **2013**, *117*, 3348−3354.
(23) Dai, S.; Fei, Z.; Ma, Q.; Rodin, A. S.; Wagner, M.; McLeod, A. S.; Liu, M. K.; Gannett, W.; Regan, W.; Watanabe, K.; Taniguchi, T.; Thiemens, M.; Dominguez, G.; Castro Neto, A. C.; Zettl, A.; Keilmann, F.; Jarillo-Herrero, P.; Fogler, M. M.; Basov, D. N. Tunable phonon polaritons in atomically thin van der Waals crystals of boron nitride. *Science* **2014**, *343*, 1125−1129.
(24) Tranca, D. E.; Stanciu, S. G.; Hristu, R.; Stoichita, C.; Tofail, S. A. M.; Stanciu, G. A. High-resolution quantitative determination of

DOI: 10.1021/acsphotonics.6b00911
ACS Photonics XXXX, XXX, XXX−XXX

dielectric function by using scattering scanning near-field optical microscopy. *Sci. Rep.* **2015**, *5*, 11876.
(25) Rajapaksa, I.; Uenal, K.; Wickramasinghe, H. K. Image force microscopy of molecular resonance: A microscope principle. *Appl. Phys. Lett.* **2010**, *97*, 073121.
(26) Rajapaksa, I.; Kumar Wickramasinghe, H. Raman spectroscopy and microscopy based on mechanical force detection. *Appl. Phys. Lett.* **2011**, *99*, 161103.
(27) Jahng, J.; Fishman, D. A.; Park, S.; Nowak, D. B.; Morrison, W. A.; Wickramasinghe, H. K.; Potma, E. O. Linear and nonlinear optical spectroscopy at the nanoscale with photoinduced force microscopy. *Acc. Chem. Res.* **2015**, *48*, 2671−2679.
(28) Jahng, J.; Brocious, J.; Fishman, D. A.; Yampolsky, S.; Nowak, D.; Huang, F.; Apkarian, V. A.; Wickramasinghe, H. K.; Potma, E. O. Ultrafast pump-probe force microscopy with nanoscale resolution. *Appl. Phys. Lett.* **2015**, *106*, 08113.
(29) Jang, J.; Ladani, F. T.; Khan, R. M.; Li, X.; Lee, E. S.; Potma, O. E. Visualizing surface plasmon polaritons by their gradient force. *Opt. Lett.* **2015**, *40*, 5058−5061.
(30) Gomez, C. J.; Garcia, R. Determination and simulation of nanoscale energy dissipation processes in amplitude modulation AFM. *Ultramicroscopy* **2010**, *110*, 626−633.
(31) Devlin, R. C.; Khorasaninejad, M.; Chen, W. T.; Oh, J.; Capasso, F. Broadband high-efficiency dielectric metasurfaces for the visible spectrum. *Proc. Natl. Acad. Sci. U. S. A.* **2016**, *113*, 10473−10478.
(32) Nowak, D.; Morrison, W.; Wickramasinghe, H. K.; Jahng, J.; Potma, E.; Wan, L.; Ruiz, R.; Albrecht, T. R.; Schmidt, K.; Frommer, J.; Sanders, D. P.; Park, S. Nanoscale chemical imaging by photoinduced force microscopy. *Science Advances* **2016**, *2*, e1501571.
(33) Wagner, T.; Beyer, H.; Reissner, P.; Mensch, P.; Riel, H.; Gotsmann, B.; Stemmer, A. Kelvin probe force microscopy for local chracterization of sctive nanoelectronic devices. *Beilstein J. Nanotechnol.* **2015**, *6*, 2193−2206.
(34) Jahng, J.; Kim, B.; Lee, S. E.; Potma, E. O. Quantitative aalysis of sideband coupling in photoinduced force microscopy. *Phys. Rev. B: Condens. Matter Mater. Phys.* **2016**, *94*, 195407.

DOI: 10.1021/acsphotonics.6b00911
ACS Photonics XXXX, XXX, XXX−XXX